Intravoxel incoherent motion modeling

Optimization of acquisition, analysis and tumor tissue characterization

Oscar Jalnefjord

Department of Radiation Physics,
Institute of Clinical Sciences at
Sahlgrenska Academy
University of Gothenburg

Gothenburg, Sweden, 2018

UNIVERSITY OF
GOTHENBURG

All models are wrong but some are useful
George E.P. Box (1979)

Abstract

Intravoxel incoherent motion (IVIM) analysis provides a means to obtain information on diffusion and perfusion from a single MRI sequence. The measurements are completely noninvasive and the results have been shown to be of interest, for example, in oncological applications. Although the use of IVIM analysis has increased substantially the last decade, choice of acquisition parameters and analysis methods are still open questions.

The aim of this thesis was to improve IVIM analysis by optimization of the image acquisition and parameter estimation methods, and to study the ability of IVIM parameters to be used for tumor tissue characterization.

With standard model-fitting methods and data quality, IVIM parameter estimation uncertainty is typically high. However, several Bayesian approaches have been shown to improve parameter quality. In Paper I, these Bayesian approaches are compared using simulated data and data from a tumor mouse model. The results emphasize the impact of methodological choices, especially the prior distribution, at typical noise levels.

Quick and robust IVIM examinations are important for clinical adoption, but consensus regarding methodology is lacking. To address this issue a framework for protocol optimization is presented in Paper III and a comparison of estimation methods was done in Paper II. To test the optimization framework, a protocol for liver examination was generated and tested on simulated data and data from healthy volunteers resulting in improved IVIM parameter quality. The compared estimation methods were evaluated on simulated data and data from patients with liver metastases with similar results for all methods, thereby making the computationally most effective method preferable.

Studies of tumors using quantitative imaging methods such as IVIM often only extract an average parameter value from the entire tumor and may thus miss important information. Paper IV explores the ability of IVIM parameters to identify tumor subregions of functionally different status using clustering methods. The obtained subregions were found to have different proliferative status as derived from histological analysis.

The work presented in this thesis has resulted in improved IVIM acquisition and analysis methods. It also shows that IVIM has the potential to provide insight into tumor physiology and be used as a noninvasive imaging biomarker.

Keywords: IVIM, MRI, diffusion, perfusion, cancer

Populärvetenskaplig sammanfattning

Magnetkameran (MR) spelar en mycket viktig roll inom medicinsk diagnostik med sin förmåga att avbilda mjukdelar i kroppen. Unikt med MR är också det stora antalet vävnadsegenskaper som kan avbildas. Bland annat kan man skapa MR-bilder där pixelvärdet är kopplat till omfattningen av mikroskopisk rörelse hos vattenmolekyler i en vävnad. I kroppen finns två viktiga typer av sådan rörelse: diffusion och mikrocirkulation.

Diffusion är slumpmässig rörelse hos vattenmolekyler som beror på deras rörelseenergi. I vävnad hindras denna rörelse av bland annat cellmembran och andra mikroskopiska strukturer. Genom att kunna mäta storleken på diffusionsrörelsen är det därför möjligt att få information om vävnadens mikrostruktur. Exempelvis kan det ge information om celltäthet och membrangenomtränglighet.

Mikrocirkulation, dvs. blodflödet genom de minsta blodkärlen (kapillärerna), är mycket viktigt för en vävnad eftersom det är genom den processen som syre och näringsämnen överlämnas till vävnaden. Eftersom syre och näringsämnen är nödvändiga för att en vävnad ska fungera kan mätning av mikrocirkulation ge information om hur en vävnad mår.

Genom att ta flera MR-bilder med varierande känslighet för mikroskopisk vattenrörelse kan man beräkna kvantitativa mått på diffusion och mikrocirkulation i en vävnad.

Denna avhandling kretsar kring mätning och analys av magnetkamerabilder känsliga för mikroskopisk vattenrörelse och hur de kan användas för karakterisering av tumörer. Målet med arbetet var att förbättra bildtagning och analys av denna typ av bilder.

För en enkel variant på avbildning, mer lämpad för en klinisk situation, togs en metod fram för optimala val av nivåer på rörelsekänslighet. Olika analysmetoder jämfördes också för att se vilken som gav mest säkra och stabila mått på diffusion och mikrocirkulation.

För en något mer tidskrävande variant på avbildning, mer lämpad för forskningsapplikationer, jämfördes analysmetoder som använder olika antaganden och som därför kan ge mer stabila mått på diffusion och mikrocirkulation. En av de studerade analysmetoderna användes sedan ihop med en nyutvecklad metod för att identifiera delregioner i tumörer med olika vävnadsegenskaper.

Avhandlingsarbetet har resulterat i förbättrad bildtagning och analys för mätning av mikroskopisk vattenrörelse med magnetkamera, särskilt för karakterisering av tumörer.

List of papers

This thesis is based on the following studies, referred to in the text by their Roman numerals.

I. **Impact of prior distributions and central tendency measures on Bayesian intravoxel incoherent motion model fitting**
Oscar Gustafsson*, Mikael Montelius, Göran Starck, Maria Ljungberg
Magnetic Resonance in Medicine 2018;79(3):1674-1683

II. **Comparison of methods for estimation of the intravoxel incoherent motion (IVIM) diffusion coefficient (D) and perfusion fraction (f)**
Oscar Jalnefjord, Mats Andersson, Mikael Montelius, Göran Starck, Anna-Karin Elf, Viktor Johanson, Johanna Svensson, Maria Ljungberg
Magnetic Resonance Materials in Physics, Biology and Medicine 2018; *In press*

III. **Optimization of b-value schemes for estimation of the diffusion coefficient (D) and the perfusion fraction (f) with segmented intravoxel incoherent motion (IVIM) model fitting**
Oscar Jalnefjord, Mikael Montelius, Göran Starck, Maria Ljungberg
Manuscript

IV. **Data-driven identification of tumor subregions using intravoxel incoherent motion**
Oscar Jalnefjord, Mikael Montelius, Jonathan Arvidsson, Eva Forssell-Aronsson, Göran Starck, Maria Ljungberg
Manuscript

*Gustafsson was the name of the author until June 2017

Related presentations

Improved IVIM model fitting with non-rigid motion correction
Oscar Gustafsson, Mikael Montelius, Maria Ljungberg
Annual Meeting ISMRM 2015 Toronto, Canada

IVIM reveals higher blood perfusion of liver metastases after oral intake of salovum
Mikael Montelius, **Oscar Gustafsson**, Mats Andersson, Eva Forssell-Aronsson, Ragnar Hultborn, Susanne Ottosson, Göran Carlsson, Stefan Lange, Maria Ljungberg
Annual Meeting ESMRMB 2015 Edinburgh, UK

An assessment of Bayesian IVIM model fitting
Oscar Gustafsson, Mikael Montelius, Göran Starck, Maria Ljungberg
Annual Meeting ISMRM 2016 Singapore

Can Cramer-Rao Lower Bound be used to find optimal b-values for IVIM?
Oscar Gustafsson, Maria Ljungberg, Göran Starck
Annual Meeting ISMRM 2016 Singapore

Impact of prior distribution and central tendency measure on Bayesian IVIM model fitting
Oscar Gustafsson, Mikael Montelius, Göran Starck, Maria Ljungberg
Annual Meeting ISMRM 2017 Honolulu, USA

IVIM D and f - Optimal estimation technique and their potential for tissue differentiation
Oscar Jalnefjord, Mats Andersson, Mikael Montelius, Göran Starck, Anna-Karin Elf, Viktor Johanson, Johanna Svensson, Maria Ljungberg
Joint Annual Meeting ISMRM-ESMRMB 2018 Paris, France

Abbreviations

ADC	Apparent Diffusion Coefficient
ASL	Arterial Spin Labeling
CRLB	Cramer-Rao Lower Bound
D	Diffusion coefficient
D^*	pseudo-Diffusion coefficient
DCE	Dynamic Contrast Enhanced
DSC	Dynamic Susceptibility Contrast
DWI	Diffusion Weighted Image/Imaging
f	perfusion fraction
GMM	Gaussian Mixture Model/Modeling
IVIM	IntraVoxel Incoherent Motion
MRI	Magnetic Resonance Imaging
NLLS	NonLinear Least Squares
S_0	Signal without diffusion weighting
sIVIM	simplified IVIM
SNR	Signal-to-Noise Ratio

Contents

Introduction

Magnetic resonance imaging (MRI) can be made sensitive to motion
through the use of magnetic field gradients. If the motion of spins
is coherent on the voxel level, it will introduce a phase offset rela-
tive to stationary tissue. On the other hand, if the motion of spins
is incoherent within a voxel, i.e. if the motion of spins varies within
the voxel, a phase dispersion is introduced that attenuates the sig-
nal in varying degree depending on the motion and how the motion
encoding was performed. One well known incoherent motion is the
self-diffusion of water molecules. The effect of diffusion on the MR
signal was early recognized [1] and was followed by development of a
method to measure it [2]. Later, diffusion sensitizing gradients were
combined with an imaging readout, which made it possible to produce
images that quantified the tissue water diffusion in vivo [3]. However,
in the same paper it was noted that a diffusion weighted image (DWI)
is not only sensitive to diffusion, but also to all other motions that
are incoherent on the voxel scale, especially blood microcirculation
or perfusion. The technique was therefore called intravoxel incoherent
motion (IVIM) imaging. Shortly after the measurement technique was
presented, a way of separately quantifying the diffusion and perfusion
was presented [4]. This quantification approach has later become syn-
onymous to IVIM, while DWI has become the standard name for the
imaging technique.

The main assumption in quantitative IVIM analysis is that the
MR signal originates from two compartments, the intravascular space
and the extravascular space, respectively. The IVIM model that is
most often used includes one parameter for describing the tissue wa-
ter diffusion (D), one for describing the motion of water molecules in
the blood (D^*) and one for the amount of blood in the voxel (f) [4].
The values of these parameters can be estimated by acquiring images
with at least four different diffusion weightings (b-values) followed by

fitting the model to the acquired data. The diffusion coefficient D is of interest since it is affected by e.g. cellularity and membrane permeability and therefore provides a means to probe tissue microstructure [5]. The perfusion-related parameters (f and D^*) are not as well-studied, but perfusion MRI in general and dynamic contrast enhanced (DCE) MRI in particular is an important diagnostic tool with its sensitivity to blood supply [6]. If IVIM based perfusion MRI can be used in at least a subset of all perfusion examinations it would be beneficial since it is completely noninvasive unlike DCE MRI that requires an intravenous injection of a contrast agent.

While appearing conceptually simple, IVIM has been shown to be nontrivial to implement in practice. The estimation of the IVIM parameters has been found to be problematic, especially for D^*, due to susceptibility to noise [7]. To improve the quality of parameter estimates, a large number of estimation approaches have been proposed, including some where only D and f are estimated [8, 9]. Improved robustness has been achieved through the use of specialized or advanced estimation approaches, but there is still little or no consensus and estimation approaches varies between studies, which reduces the comparability between studies.

In addition to using a specifically designed estimation approach, choosing optimal b-values has a potential to reduce the uncertainty of parameter estimates substantially. Methods for experiment design have been applied successfully to several aspects of diffusion-weighted imaging including IVIM [10–13]. However, the optimal choice of b-values may dependent on the estimation approach. Most work on b-value optimization for IVIM has been focused on a generic simultaneous estimation of all model parameters, while optimization of b-values for other more specialized estimation approaches is mainly unexplored. For example, estimation limited to D and f is attractive in a clinical setting due to its short acquisition and processing time, and robustness, but optimization of b-values for this approach has only been studied for a special case [14, 15].

With its ability to quantitatively map both diffusion and perfusion, IVIM has been proposed as an interesting diagnostic tool in several oncological applications [16]. Tumor tissue characterization based on quantitative imaging, such as IVIM, has a great potential to, for example, improve the understanding of tumor development by repeated imaging either during growth or after therapy. However, even though it is well known that tumors can be highly heterogeneous and that

quantitative imaging can provide potentially important spatial information, parameter values are often averaged across the entire tumor [17]. To obtain more information, it has been proposed to do separate analyses in smaller subregions of the tumor. By doing so, spatial information is provided in a way that is relatively easy to interpret. Such subregions can be defined, for example, based on geometrical properties like distance from the center or based on functional characteristics derived from the parameter maps. With both diffusion and perfusion parameter maps, IVIM is an interesting candidate for such a functional definition of tumor subregions.

Aims

The overall aim of this thesis was to improve intravoxel incoherent motion (IVIM) analysis, especially for tumor tissue characterization. The specific aims of the papers included in the thesis were:

- to evaluate the impact of estimation approach both for the full IVIM model (Paper I) and for the analysis restricted to the parameters D and f (Paper II)

- to develop and evaluate a framework for optimization of b-value schemes for DWI data used to estimate the parameters D and f (Paper III)

- to investigate if clustering based on IVIM parameter maps can be used for identification of tumor subregions with biological relevance (Paper IV)

Intravoxel incoherent motion (IVIM)

The IVIM concept

The principle for diffusion weighted imaging is that nonstationary spins gain a phase offset relative to stationary spins due to the diffusion encoding. The obtained phase depends on the trajectory traversed by the spin during the diffusion encoding and may therefore differ between spins within a voxel. For an incoherent motion, i.e. if all spins do not move in a single straight line with the same speed, the result is a phase dispersion and therefore a reduced amplitude of the signal. The incoherence can be due to motion in different directions by different spins (spatial incoherence), motion in different directions by the same spin (temporal incoherence) or a combination of both [4, 18]. The resulting signal attenuation of the diffusion weighted signal depends on the characteristics of the incoherent motion as well as the technique used for diffusion encoding. To emphasize that it is motions that are incoherent on the voxel level, these kinds of motion are called intravoxel incoherent motion (IVIM).

For in vivo MR imaging there are two major types of IVIM's that affect the diffusion weighted signal. These are tissue water diffusion and blood microcirculation.

Diffusion is a random motion that is driven by the kinetic energy of the particles, in this case water molecules. During a typical encoding time of tens of milliseconds a water molecule collides and changes directions on the order of 10^{10} times [19]. The motion of the molecules can therefore be seen as a random walk with multiple steps taken during the diffusion encoding, with different trajectories for different water molecules (left illustration in Figure 1). In tissue, the diffusion

can be hindered or restricted by structures such as cell membranes and organelles, which reduces the distance covered by the water molecules. The reduced magnitude of the diffusion can therefore be used to probe tissue microstructure through diffusion weighted MRI.

Microcirculation is the flow of blood in the capillaries, also referred to as perfusion in this thesis. While the motion of water molecules due to blood flow is not necessarily an incoherent motion, it is reasonable to assume that the capillaries contained in a typical voxel (side 2-3 mm) are not perfectly aligned but rather arranged in many directions (right illustration in Figure 1). The variable orientation of capillaries is a source of spatial incoherence, which makes the microcirculation an IVIM. Depending on the capillary architecture, blood velocity and duration of the diffusion encoding, microcirculation can also give rise to temporal incoherence [4]. In such case, microcirculation has an equivalent effect on the MR signal as diffusion and has therefore been called pseudo-diffusion. Assuming temporal incoherence simplifies the signal modeling (see below) and is therefore used in most studies, but it is still unclear in what measurement situations that the assumption holds. The assumption has, for example, been shown to be violated in the brain [18] and the liver [20]. However, the commonly used model usually fits well to data and the major implication that this violation on the assumption has is therefore to make the interpretation of some, but not all, model parameters less straight forward. One can, for example, end up with parameter estimates that are highly dependent on the choice of b-values [18]. Nevertheless, if appropriate measurement methods and analysis are used, the effect of blood microcirculation on the diffusion weighted signal enables extraction of perfusion information from DWI regardless of capillary architecture [4].

The IVIM model

The overall assumption for IVIM analysis is that the MR signal originates from two compartments: the intravascular space and the extravascular space, which have individual response to diffusion encoding [4]. The two compartment are also referred to as the perfusion compartment and the diffusion compartment, respectively, in this thesis based on the most influential IVIM in the particular compartment. To separate the effects of diffusion and perfusion on the diffusion weighted MR signal a model can be formulated as follows:
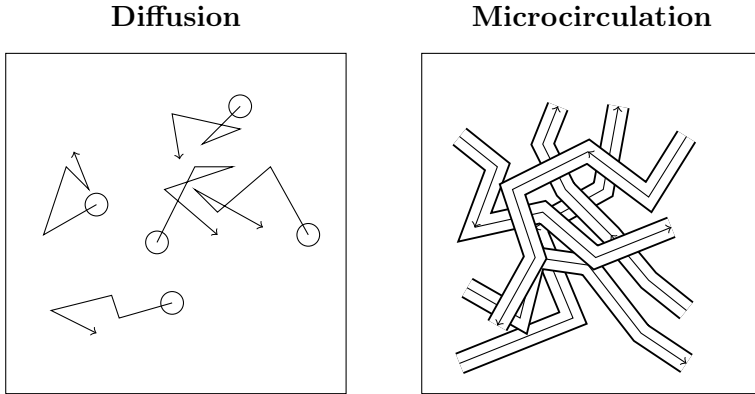
Figure 1: Illustration of the two major sources of intravoxel incoherent motion in living tissue: water diffusion and microcirculation
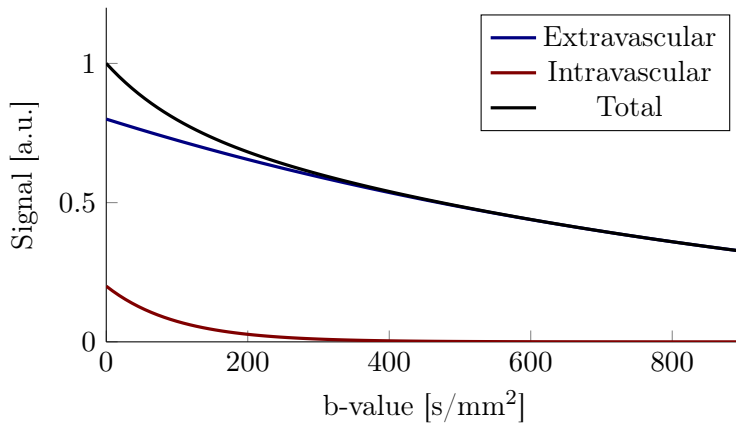

Figure 2: An example IVIM signal vs. b-value curve. The curves show the signal from each compartment and their sum, which is what is measurable. Data was generated using Equation 3 with parameter values: $S_0 = 1$, $D = 1$ $\mu m^2/ms$, $D^* = 10$ $\mu m^2/ms$, $f = 0.2$

$$S_b = S_0 \left((1 - f) F_D + f F_P \right) \tag{1}$$

where S_b is the signal at b-value b, S_0 is the signal without diffusion weighting, f is the signal fraction originating from the intravascular space (referred to as perfusion fraction), and F_D and F_P are functions that describe how the signal is attenuated by the diffusion weighting in the extravascular and intravascular spaces respectively. In most cases, the signal decay due to diffusion weighting is stronger in the perfusion compartment. This results in a signal vs. b curve where the initial slope is dominated by perfusion effects, and the latter parts by diffusion effects (Fig. 2).

For weak to intermediate magnitudes of the diffusion weighting (b-values less than approximately 1000 s/mm^2), the signal attenuation in the extravascular space is well approximated by a monoexponential function [19]. Equation 1 can therefore be written as:

$$S_b = S_0 \left((1 - f) e^{-bD} + f F_P \right) \tag{2}$$

where D is the diffusion coefficient in the extravascular space. This is the form that was originally proposed by le Bihan et al. [4]. More recent work has extended that model to include the effects of diffusional variance by the use of e.g. the kurtosis model [16]. However, studies of such extensions are beyond the scope of this thesis.

Remaining to be determined in Equation 2 is the effect of diffusion weighting on the intravascular space (F_P). However, since temporal incoherence is not necessarily a valid assumption it can be a non-trivial task to describe F_P. The two special cases of no temporal incoherence and full temporal incoherence was described by le Bihan in the original paper. The intermediate case is yet an open topic for research where some attempts have been made that warrants further research [20, 21].

In the case of full temporal incoherence, it is assumed that the capillary architecture and the blood flow is such that the water molecules in the blood changes direction a sufficient number of times during the diffusion encoding [4]. The motion of water molecules can then be approximated by a random walk similar to the case of diffusion and F_P can be described by a monoexponential function. This results in the following IVIM model:

$$S_b = S_0 \left((1 - f) e^{-bD} + f e^{-bD^*} \right) \tag{3}$$

10

where D^* describes the motion of the blood water. Due to the pseudo-diffusion like motion of microcirculation under these circumstances, D^* is referred to as the pseudo-diffusion coefficient. Even though the assumption of temporal incoherence cannot be said to hold in general, and has been proved invalid in some studies [18, 20], the biexponential model is currently the by far mostly used IVIM model.

An alternative approach is to avoid the b-value range where F_P is not well known. Specifically, one can exploit the stronger signal attenuation in the perfusion compartment and choose to use b-values where F_P is either 1 ($b = 0$) or of negligible size ($b > b_{thr}$, where b_{thr} is some threshold b-value). This gives the simplified IVIM (sIVIM) model:

$$S_b = S_0 \left((1 - f) \, e^{-bD} + f \delta(b) \right) \tag{4}$$

where $\delta(x)$ is the discrete delta function, i.e. $\delta(x = 0) = 1$ and $\delta(x \neq 0) = 0$ [22–24]. Since the low b-values > 0 are avoided, no information can be obtain regarding the blood flow by e.g. D^*, but f is still possible to estimate if $S(0)$ is measured. Note that this simplified IVIM model does not attempt to describe the signal attenuation in the full range of b-values, but rather to provide a simple model that can be used for estimation of at least a subset of the IVIM parameters.

Relation to other MR perfusion techniques

IVIM is just one of several techniques that can be used to measure perfusion with MRI. The more commonly used techniques are dynamic contrast enhancement (DCE), dynamic susceptibility contrast (DSC) and arterial spin labeling (ASL). The techniques have different benefits, but a major advantage for IVIM and ASL is that they do not depend on an injection of a contrast agent. This is especially beneficial for patients with renal dysfunction and for small children [16].

Since diffusion weighting sensitizes the MR images to motion, the perfusion information attainable via IVIM analysis is related to the blood that is flowing [25]. This means that IVIM in principle can be used to quantify blood flow and volume of flowing blood. In fact, under some very specific conditions, it is possible to translate the IVIM perfusion parameters f and the product $f \times D^*$ into measures of blood volume and blood flow, respectively [25].

Several studies have been conducted with the aim to study the relationship between IVIM derived measures of blood volume and blood flow, and corresponding measures obtained from the other MR perfusion techniques, but the results are inconclusive [26]. Multiple studies have found correlations between f and blood volume derived from DSC and DCE [27–30], but contradicting results exist as well [30–32]. Some studies have compared $f \times D^*$ with measures of blood flow from DSC [27] and ASL [30, 33], but the data available is scarse and mainly contradicting. The relationship between IVIM perfusion parameters and measures of blood volume and blood flow from other MR perfusion techniques is thus still an open field of research [26].

There are several possible explanations for the currently poor agreement between perfusion parameters derived from IVIM and other MR techniques. On the IVIM side, there are difficulties associated with both f and D^*. f is a signal fraction, so to get something similar to a blood volume, one needs to compensate for relaxation (T1 and T2) and possibly also other factors such as contamination by cerebrospinal fluid [34, 35]. D^* on the other hand is given in absolute units, but is often strongly affected by noise [7] and is only easily interpreted under certain conditions (temporal incoherence) [18]. Different MR perfusion techniques can also be sensitive to different kinds of blood flow which complicates the comparison further [26]. Future studies on this topic should try to compensate for these confounding factors in order to facilitate more direct comparisons.

The use of IVIM

After some initial interest [36], perfusion evaluation by IVIM analysis did not gain much attention until the start of the current decade (Fig. 3). After Luciani et al. showed that IVIM analysis could be used for diagnostic purposes of liver cirrhosis [37], the IVIM field gained renewed attention [38] and the number of publications has since increased exponentially (Fig. 3).

During this decade, IVIM analysis has been applied successfully in various organs, often with oncological applications [16, 26]. It has, for example, been shown that f can be helpful in grading gliomas [29] and that both D and f provide important information for stroke assessment [39, 40]. In addition to applications related to liver cirrhosis [31, 37], IVIM has also been used in the liver for, e.g., grading of hepatocellular carcinomas [41]. IVIM parameters have also been used for
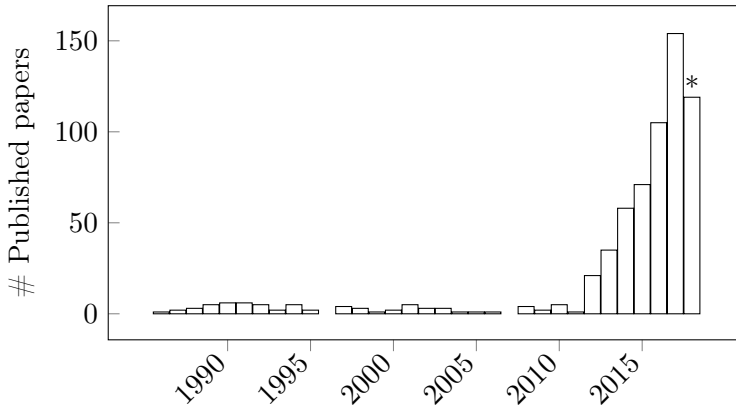
Figure 3: Number of IVIM papers published each year since the first in 1986. The data was obtained from a PubMed search with search string: "intravoxel incoherent motion" OR "IVIM". *Note that the number of published papers in 2018 is only until July 16. An extrapolated number for 2018 is 220

differentiation of common malignant pancreas tumors with promising results [42]. Another promising application of IVIM is breast cancer, where a difference in both D and f between benign and malignant tumors has been shown [43].

IVIM parameter estimation

This chapter is mainly related to Papers I and II.

In Paper I, the impact of methodological choices related to Bayesian estimation of IVIM parameters based on the biexponential model were studied. Estimation with different prior distributions and central tendency measures used in previous studies were compared.

In Paper II, methods for estimation of D and f were compared. Segmented model fitting was evaluated among with fitting of the sIVIM model based on either least squares or Bayesian methods with different central tendency measures.

Estimation of model parameters is typically done by fitting the specific model to a set of data. Therefore, parameter estimation and model fitting have equivalent meaning and will be used interchangeably in this text. Parameter estimation is often based on the maximum-likelihood method and in particular using the least-squares criterion, although other methods such as Bayesian estimation can be useful in some applications.

Maximum likelihood

Parameter estimates based on the maximum-likelihood method are obtained by finding the parameter values that maximizes the likelihood function, where the likelihood function describes the probability of the data given the set of model parameters. To formulate the likelihood function, one needs to choose a signal model and a noise model. For the work presented in this thesis, the signal model is one of the versions of the IVIM model (Eq. 3 or 4). Since magnitude images are used in general for DWI, the noise distribution is often assumed to be Rician [44]. To simplify model fitting, the signal-to-noise ratio (SNR)

is typically assumed to be high enough such that the Rician distribution can be approximated by a Gaussian one. For a single data point, this gives:

$$P(S(b)|\boldsymbol{\theta},\sigma) = \frac{1}{\sqrt{2\pi\sigma^2}} \exp\left[-\frac{(S(b) - S_b(\boldsymbol{\theta}))^2}{2\sigma^2}\right] \qquad (5)$$

where $P(S(b)|\boldsymbol{\theta},\sigma)$ is the probability density function describing how the measured value $S(b)$ varies around the predicted value S_b given the signal model parameters $\boldsymbol{\theta} = [S_0, D, f, D^*]$ and the noise variance σ^2 [45]. Furthermore, if data points in a measurement series are also (conditionally) independent, the likelihood function is given by:

$$L(\boldsymbol{\theta}) = P(\boldsymbol{S}|\boldsymbol{\theta},\sigma) = \prod_{i=1}^{N} P(S(b_i)|\boldsymbol{\theta},\sigma) =$$

$$= \left(2\pi\sigma^2\right)^{-N/2} \exp\left[-\frac{\sum_{i=1}^{N} (S(b_i) - S_{b_i}(\boldsymbol{\theta}))^2}{2\sigma^2}\right] \qquad (6)$$

where N is the number of measurements [45]. It is clear that maximization of the likelihood function with respect to the signal model parameters is achieved by minimizing the sum in the exponent. The maximum-likelihood estimate, given these specific noise assumptions, is therefore given by the so-called least-squares estimate.

Least squares

Parameter estimation based on least-squares fitting is by far the most commonly used. For linear models, closed-form solutions exist and the method is therefore very robust for such models. On the other hand, for nonlinear models, such as the IVIM model, closed-form solutions do not exist and iterative optimization methods have to be used. This leads to increased numerical complexity and decreased robustness since multiple local maxima may exist in the likelihood function.

Nonlinear least squares (NLLS) fitting of the biexponential IVIM model (Eq. 3) is very commonly used and may appear attractive since few explicit assumptions are made and it is easy to perform with routines available in most software packages. However, it was early shown to be susceptible to noise [46], a result that has been confirmed

several times since then [7–9]. The possibly most important reason for the noise sensitivity of the biexponential model is its flexibility. An over-ability to fit well to data becomes problematic if the measured signal at some key b-value is strongly influenced by noise or some artefact. Furthermore, if the perfusion fraction is small and the noise level is high, data may be very well described by a monoexponential model. Unless D and D^* are constrained to not overlap, D^* may take the role of D while f takes extremely high values or D^* and D take similar values while f can take any value in the allowed range. Given its limited robustness, NLLS for fitting of the biexponential IVIM model should therefore be avoided unless the data is of very high quality, especially for tissues with a low perfusion fraction.

The simplified IVIM model (Eq. 4) can also be fit using NLLS [22]. The model is less flexible than the biexponential model and is therefore less susceptible to noise as shown in Paper II and previously by others [9]. Nevertheless, it is a nonlinear model with multiple parameters and therefore requires iterative estimation methods, which may be computationally expensive compared with other methods.

Segmented fitting

To increase the robustness of the IVIM parameter estimates, a step-wise procedure was proposed that is often referred to as segmented or asymptotic model fitting [46]. The rationale behind the method is that one can typically assume that the diffusion weighting attenuates the signal from the perfusion compartment more strongly than that from the diffusion compartment. The result is that the term F_P in Equation 2 can be assumed to be of negligible size at a sufficiently high b-value, equivalent to the argument used to formulate the sIVIM model (Eq. 4). If the biexponential IVIM model is used, this assumption is often expressed as $D \ll D^*$. If the assumption holds ($F_P \approx 0$) and only b-values above the chosen threshold are used, the signal model simplifies to:

$$S_b = S_0 \left(1 - f\right) e^{-bD} = A e^{-bD} \tag{7}$$

This monoexponential model is fitted to get an estimate of D. The estimate of D can then be fixed in a NLLS fit where all b-values are used and the remaining IVIM parameters are estimated. Alternatively, if images with the b-value $b = 0$ have been acquired, they may be used together with the extrapolated y-axis intercept A to get an estimate

of f as:

$$f = 1 - A/S_0 \tag{8}$$

where S_0 has been set to the measured value $S(0)$. Both D and f can then be fixed in the NLLS fit where D^* is estimated. If f is estimated through the extrapolation step, the last step with estimation of D^* might be skipped while information on both diffusion and perfusion is still obtained. This reduces scan time since fewer b-values are needed as well as computational time since the NLLS step for D^* is avoided. In fact, a special case of the segment fitting approach with only three b-values was the one proposed for estimation of D and f in the original IVIM paper [4]. When only three b-values are used, closed form solutions exist for both D and f as shown in Paper III.

The segmented fitting has been compared with the simultaneous least-squares estimation of all IVIM parameters from the biexponential IVIM model in several studies [9, 47–50]. It is clear from these results that the segmented approach is preferable, with the caveat that a proper threshold b-value must be chosen.

In Paper II, segmented fitting for estimation of D and f was compared with fitting the sIVIM model (Eq. 4) using either least squares or Bayesian methods. The estimation approaches were compared regarding estimation variability and bias as well as ability to differentiate between tumor and healthy liver. Apart from some minor differences, it was found that all approaches produced very similar results (see example in Figure 4). The major difference between the approaches is instead that the segmented fitting is associated with a substantially lower computational cost and is easier to implement due to the simple stepwise procedure. In fact, segmented fitting could easily be fit into a clinical workflow where parameter maps are generated directly as an extension to the reconstruction. The conclusion from Paper II is therefore that the segmented fitting approach is preferable for estimation of D and f only.

Bayesian parameter estimation

A more general way to incorporate prior knowledge into the model fitting procedure is to take a Bayesian perspective. Instead of simply finding the parameter values that maximizes the likelihood function, the posterior parameter distribution is derived through Bayes' rule and used to obtain the parameter estimates. According to Bayes' rule, the
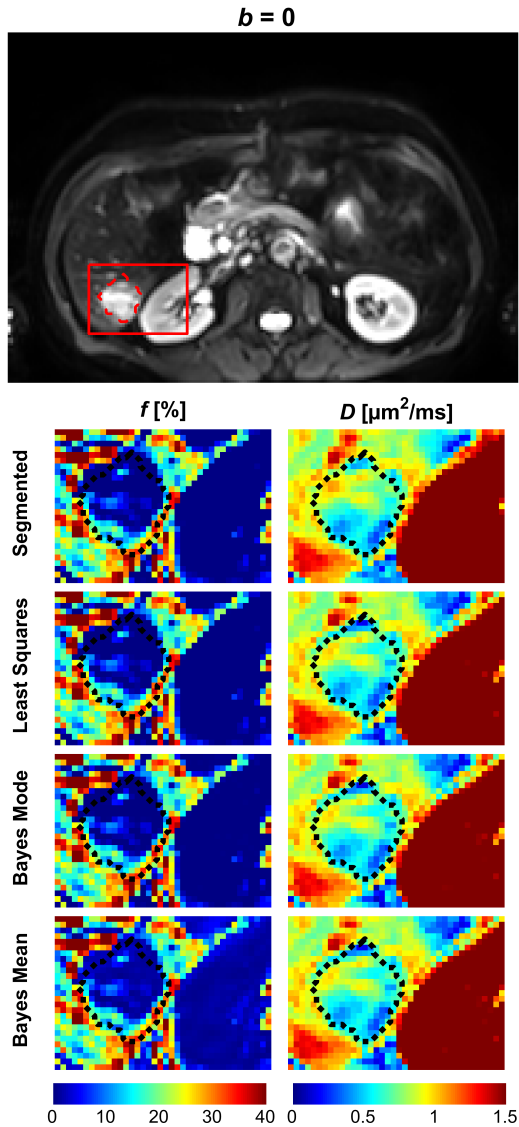
Figure 4: $b = 0$ image and IVIM parameter maps of a patient with a liver metastasis. The parameter maps are based on all estimation approaches studied in Paper II. The manual delineation of the tumor is shown as a dashed line (red in $b = 0$ image and black in parameter maps). Note that the parameter maps based on different estimation approaches are almost indistinguishable. Subtle differences can be seen, for example, in the upper left region of the D maps. Adapted from Paper II, Figure 3 with data from another patient

posterior distribution is given by:

$$P(\boldsymbol{\theta}|\boldsymbol{S}) \propto P(\boldsymbol{S}|\boldsymbol{\theta})P(\boldsymbol{\theta}) \tag{9}$$

where $P(\boldsymbol{\theta}|\boldsymbol{S})$ is the posterior distribution and $P(\boldsymbol{\theta})$ is the prior distribution [45].

Bayesian model fitting was early proposed as a robust alterative to NLLS for IVIM parameter estimation [51]. However, the computational cost associated with Bayesian methods and perhaps also the lower familiarity with such methods have resulted in limited use. Due to the continued development of computer hardware, the computational cost is currently less of a problem, but the lack of availability of simple Bayesian methods in standard software packages still limits the use[1]. One reason for the high computational cost is that analytical forms of the posterior distribution only exist for a few specific combinations of likelihood function and prior distribution, but in these cases the Bayesian estimation problem is essentially equivalent to a maximum likelihood estimation [52]. However, use of these specific prior distributions is not necessarily the most preferable.

Prior distribution

The prior distribution is used to describe what can be known about the model parameters without seeing the data of the specific experiment. Such information is, for example, that some parameters are nonnegative or even constrained to a closed interval, such as f that is defined to be in the range $0 - 1$. However, one may also include less well defined information such as a belief that D is typically around 1 $\mu m^2/ms$. By doing so, the parameter estimates may become less susceptible to noise, but they may on the other hand also become biased. Choice of prior distribution for Bayesian IVIM parameter estimation has varied between studies [8, 51, 53–57]. The impact of this choice has recently been studied both for prior distributions that act on each voxel independently (Paper I) as well as for prior distributions that take into account information from other voxels [57]. The results in both studies have shown substantial effects on parameter estimates due to the choice of prior distribution and also emphasize the need to challenge proposed methods by testing them in new situations.

---

[1]To partially remedy this issue and enable the use of Bayesian methods to a larger group, the MATLAB code used for Bayesian IVIM model fitting in Paper I has been published online:
www.mathworks.com/matlabcentral/fileexchange/65579-ivim-model-fitting

In Paper I, three prior distributions previously used for Bayesian IVIM model fitting of the biexponential IVIM model were compared. The three prior distributions were all uniform for f and S_0, but either uniform [8, 56], reciprocal [51] or lognormal [53] for D and D^*. The uniform distribution implies that any given interval of parameter values is equally likely on a linear scale. For example, a uniform prior gives equal probability for values in the range 1 - 2 as for values in the range 2 - 3. The reciprocal distribution has the equivalent meaning on a log-scale. This means that the reciprocal prior, for example, gives equal probability for values in the range 1 - 10 as for values in the range 10 - 100. The lognormal priors used in Paper I were normal distributions on the log-scale with relatively high variance. All investigated priors can therefore be described as non-informative or weakly informative since no or only very little information is provided by the priors. This is in contrast to, for example, a lognormal prior with low variance implying a strong belief for a specific narrow range of parameter values. The comparison in Paper I showed that the reciprocal prior tended to dominate the posterior distribution at SNR levels below 40 (Fig. 5). At SNR levels around 20, which are typical levels for IVIM, at least in applications outside the brain, the parameter estimates were therefore strongly biased (Fig. 6). Worth noting is that the first study on Bayesian IVIM model fitting used the reciprocal priors [51], but only tested for SNR levels of 40 or higher where such a prior is less dominant and this negative effect was therefore not observable. The other two prior distributions, i.e. uniform and lognormal, produced more similar results except for estimates of D^*, where the spuriously high values that are typically produced by noise corruption were strongly suppressed by the use of lognormal priors. The resulting D^* parameter maps were of subjectively high quality although it should be noted that it is unclear what the magnitude of the bias on the obtained parameters was (Fig. 6). The conclusion from Paper I was that the reciprocal prior needs unrealistically high SNR to be useful, while the other two compared priors have comparable performance. The lognormal prior necessitates choice of distribution parameters (mean and variance) and is therefore somewhat more subjective, but appears to have slightly lower demands on noise level for estimation of D^*. The uniform prior on the other hand, has no distribution parameters and may therefore be regarded as more objective, but appears to be somewhat more susceptible to noise which is demonstrated especially for D^*. The specific choice of prior distribution for
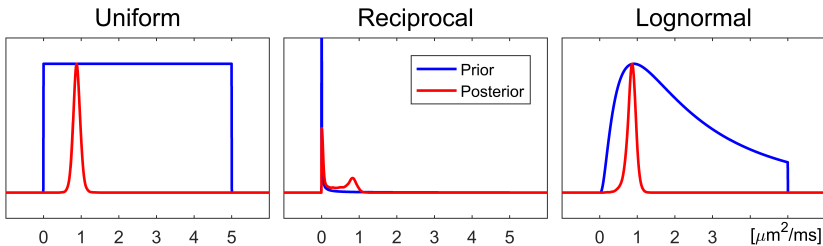
Figure 5: Posterior distribution for D based on simulated data with SNR = 20 for different prior distributions (uniform, reciprocal or lognormal). The posterior distribution is strongly dominated by the reciprocal prior, but mainly unaffected by the other priors. The data was scaled to improve visibility. Adapted from Paper I, Figure 2 with permission from John Wiley & Sons, Inc.

Bayesian IVIM model fitting should be made with these aspects in mind and the optimal choice typically depends on the specific context.

Only the uniform prior was used in Paper II. Due to the reduced flexibility of the sIVIM model compared with the biexponential IVIM model, it was believed that the choice of prior distribution would be less important.

Measures of central tendency

To arrive in a parameter estimate, the posterior distribution must be summarized by some central tendency measure. A simple approach is to find the parameter values that maximize the joint posterior distribution similar to maximum likelihood estimation [52]. However, for Bayesian IVIM parameter estimation it has been more common to find the marginal posterior distributions, i.e. $P(D|\boldsymbol{S})$, $P(f|\boldsymbol{S})$ and $P(D^*|\boldsymbol{S})$. From these marginal posterior distributions, parameter estimates have been obtained by calculation of the mean [53, 55] or the mode, i.e. the parameter value where the marginal posterior distribution has its maximum [8, 51].

In Papers I and II parameter estimates based on the mean or the mode were compared for the biexponential IVIM model (Eq. 3) and the sIVIM model (Eq. 4), respectively. The results showed that the choice of central tendency measure has an impact on the resulting parameter estimates, but that it is of limited magnitude (Figs. 4 and 6). The most prominent differences could be seen when the true parame-
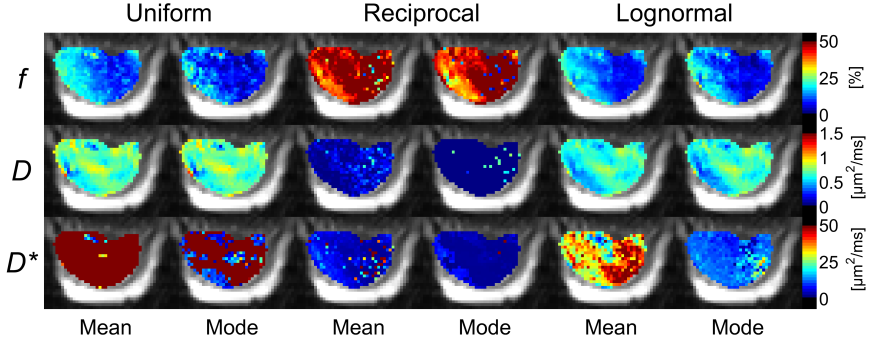
Figure 6: IVIM parameter maps (color) of a neuroendocrine tumor of the GOT1 tumor model [58] overlaid on the $b = 0$ image (grayscale). The parameter maps were obtained with different combinations of prior distributions (uniform, reciprocal or lognormal on D and D^*, and uniform on f and S_0) and central tendency measures (mean or mode). The reciprocal prior distribution produced parameter maps that were strongly affected by the prior. Adapted from Paper I, Figure 3 with permission from John Wiley & Sons, Inc.

ter value was close to a parameter boundary such as for small values of f. In those cases, the posterior distribution is often strongly skewed which gives a noticeable difference between the mean and the mode, and the typical result is a positive bias of parameter estimates based on the mean. In Paper I it was also shown that for the biexponential IVIM model, the choice of central tendency measure is not as critical as the choice of prior distribution, but still may impact the results in some specific cases, e.g. estimation of D^* with a uniform or lognormal prior (Fig. 6).

Optimization of b-value schemes for IVIM

This chapter is mainly related to Paper III.

In Paper III, a framework for optimization of b-value schemes was presented and evaluated. The framework was used to create a b-value scheme for examination of healthy liver, which was compared with linearly distributed b-values.

A key aspect of an IVIM experiment is the choice of b-values. The optimal choice depends of factors such as specific model, expected parameter values, noise level and purpose of analysis. A commonly used strategy is to define an objective measure to describe how good a b-value scheme is and then maximize this measure by finding the optimal b-values. The definition should take into account all aspects that are considered important and combine them into a single figure of merit. The way that the goodness of a b-value scheme is summarized into a single number is typically referred to as the objective function.

Objective function

The objective functions used for experiment design, such as choice of b-value, are typically based on some measure of estimation variability for the parameters of interest. Note that in such case, the objective function should be minimized rather than maximized in order to obtain a b-value scheme that minimizes the estimation variability. A simple objective function for analysis of the biexponential IVIM model

could be:

$$O = \sum_{p \in \{D, f, D^*\}} c_p \sigma_p \tag{10}$$

where σ_p is the estimation variability of the parameter p and c_p is a scaling constant used to set the σ_p's on the same scale. A common choice is to set $c_p = 1/p$, which turns Equation 10 into a sum of coefficients of variation if the σ_p's are standard deviations, but the c_p's can in principle be set to any values of choice. Although S_0 is a parameter of the IVIM model it is usually not included in the sum in an objective function like this since it is typically not of interest.

The exact type of estimation variability and how to combine them when multiple model parameters are of interest such as in the case of IVIM, is a subjective choice. In Paper III and some other studies on optimization of b-value schemes for IVIM [12, 50, 59], a sum of coefficients of variation (as in Eq. 10) was used, but other choices are reasonable as well. Some examples, used for experiment design in diffusion MRI, are weighted sums of estimation variance [11] and median absolute percentage deviation [14]. As discussed in Paper III, no measure can be considered generally superior, but the choice will have an impact on the obtained b-value scheme. It is therefore important to consider the strengths and weaknesses of the potential measures when designing the objective function and make a choice that fit well to the particular application of interest.

Most often it is not enough to provide knowledge about the model and typical model parameter values to the objective function, but restrictions on the experiment parameter, i.e. the b-values, and indirect effects related to them may also be needed. An important example of such restrictions for IVIM is that b-values are nonnegative, and for the sIVIM model it is also necessary to have both $b = 0$ and at least two different b-values in a higher interval above the threshold. One may also take into account the increased echo time, and thereby reduced SNR, for higher b-values that is caused by limited gradient performance as done in Paper III and previously by others [11, 13]. With simplified models, some intervals of b-values may be poorly described by the model. Examples are low b-values for the sIVIM model and high b-values for all models with only a monoexponential term for the diffusion compartment. Such unfavorable b-values should be avoided in order not to introduce a potential estimation bias. Furthermore, if there are any additional assumptions for the model to be valid, it is important to design the optimization such that these assumptions are

not violated. It is, for example, often assumed that the SNR is sufficient for a Gaussian noise approximation, which is not necessarily true at high b-values. To take all this into account, one can perform a constrained optimization or add penalty terms to the objective function such that b-value schemes that violate some assumption or restriction are associated with a large penalty. Typically a combination of both is used, i.e. constrained optimization of an objective function with penalty terms. The exact implementation depends on what is considered most suitable for the particular optimization.

To evaluate the objective function it is necessary to be able to calculate all of its components. There exist two general ways of obtaining these values; either by expressions derived from theory, which are fast and relatively simple to calculate, or by experiment-like approaches such as simulations, which are slower, but more closely related to the actual measurement procedure.

Expression-based approaches

Expression-based approaches typically use some theory to derive an expression of the estimation variance based on the model, experiment design and noise properties. For diffusion MRI, the most commonly used approaches are error propagation and Cramer-Rao lower bound [10–13, 59–63].

Error propagation

If closed form solutions exist for all model parameters of interest, it is possible to use error propagation to find the variance of parameter estimates. For independent measurements, the error propagation is given by:

$$\sigma_{\theta_j}^2 = \sum_{i=1}^{N} \sigma_i^2 \left(\frac{\partial \theta_j}{\partial S_{b_i}} \right)^2 \tag{11}$$

where $\sigma_{\theta_j}^2$ is the estimation variance of parameter θ_j and σ_i^2 is the variance of the noise of the ith measurement [45].

Error propagation has, for example, been used to find optimal b-values for estimation of the apparent diffusion coefficient (ADC) based on the monoexponential diffusion model [10, 61]. In Paper III, it is shown that error propagation can be used to obtain optimal b-values

for estimation of D and f based on segmented model fitting and a protocol containing three unique b-values.

Cramer-Rao lower bound

When the number of measurements is higher than the number of parameters in the model, parameter estimation is typically done by least squares. In this case, the standard method for error propagation presented above cannot be used. Instead a similar method called Cramer-Rao lower bound (CRLB) can be used. The CRLB's are theoretical lower bounds of the parameter estimation variances. Minimizing these bounds has the potential to result in lower estimation variability. The CRLB's are given by the diagonal elements of the inverse Fisher matrix as:

$$\sigma_{\theta_j}^2 \geq (F)_{jj}^{-1} \tag{12}$$

where the elements of the Fisher matrix are given by [45]:

$$F_{jk} = -E\left[\frac{\partial^2}{\partial \theta_j \partial \theta_k} \log L\left(\boldsymbol{\theta}\right)\right] \tag{13}$$

If the likelihood function $L(\boldsymbol{\theta})$ is based on a Gaussian noise model (Eq. 6), the expression simplifies to the following [11]:

$$F_{jk} = \frac{1}{\sigma^2} \sum_{i=1}^{N} \frac{\partial S_{b_i}(\boldsymbol{\theta})}{\partial \theta_j} \frac{\partial S_{b_i}(\boldsymbol{\theta})}{\partial \theta_k} \tag{14}$$

CRLB based methods have been used for optimization of acquisition parameters for several applications of diffusion MRI, e.g., kurtosis imaging [64], filter exchange imaging [13] and biexponential IVIM [12, 50, 59].

In Paper III, a CRLB-based method was used to find optimal b-value schemes for estimation of D and f based on segmented model fitting, without the limitation of only three unique b-values. Specifically, a b-value scheme designed for imaging of the liver was optimized. Although additional b-values were allowed, the optimized b-value scheme contained no more than three unique b-values. These three b-values were instead repeated if more acquisitions were allowed. The optimal ratio of repetitions was found to be approximately 1:2:2 for a scheme containing b-values 0, 200 and 800 s/mm^2. This should be contrasted to the ratio 1:3 that is considered optimal for the monoexponential diffusion model and b-values 0 and 1000 s/mm^2 [10], and the ratio

1:2:2:1 for the biexponential IVIM model (Eq. 3) and b-values 0, 15, 100 and 1000 s/mm^2 [65]. Optimal signal averaging is thus highly dependent on the model that is used.

When compared with linearly distributed b-values, simulations in Paper III showed that the estimation variability could be reduced by about 20 % by the use of an optimized b-value scheme. These results were confirmed in vivo using data from healthy volunteers (see example in Figure 7). A critical issue when D and f are to be estimated is to find the threshold b-value where the signal contribution from the perfusion compartment can be considered negligible. Notably, the results in Paper III showed that the decrease in estimation variability could be seen regardless of if the threshold was chosen properly or not.

The observation in Paper III that the optimized b-value scheme contained only three unique b-values is in line with what has been reported previously by others [12, 59, 63], i.e. that optimization based on CRLB tends to produce b-value sets where the number of unique b-values equals the number of parameters included in the model. If three b-values were considered sufficient for the estimation of D and f based on segmented model fitting, closed form expressions exist for both parameters, and it would thus be possible to use optimization methods based on error propagation. The result would be simpler expressions for estimation variability, which can be interpreted more easily, and less complicated optimization since the number of free parameters is reduced.

Experiment-like approaches

The major drawback of expression-based approaches for experiment optimization is that some aspects can be hard to incorporate into a closed form expression. A more straight-forward approach is to compare direct measures of the quality of results from measurements done with different experiment design. However, if these experiments would include actual MR scanning only a very limited number of designs can be tested [12]. A faster and cheaper way to generate data is to do computer simulations. Simulation-based approaches are attractive in the sense that they are easily understood and closely resemble the actual experiment that is to be optimized. To obtain the error terms included in the objective function, two steps are used: generation of noisy data based on some signal model, noise distribution and experiment design, and parameter estimation based on the noisy data with the model of

choice, which is not necessarily the same as was used for data generation. This simplicity is in contrast to expression-based approaches where the effect of these two steps must be described explicitly.

Simulation-based approaches have been used in IVIM applications to find optimal b-values for the biexponential IVIM model in various organs [7] and to find an optimal intermediate b-value in a three-b-value examination used to estimate D and f [14, 15]. However, the computational cost is significant to evaluate the objective function, especially if closed form expressions for parameters do not exist. This has resulted in somewhat simplified optimization approaches. To reduce the number of free parameters in the optimization Lemke et al. chose to build the b-value schemes incrementally by adding additional b-values one-by-one [7]. Doing so may produce b-value schemes that are suboptimal as a whole, since the added b-value is only optimal given the already fixed b-values. While et al. and Meeus et al. chose to only optimize the intermediate b-value, which enabled an exhaustive search, but the upper b-value was fixed in the optimization [14, 15]. The obtained results are therefore dependent on the preset upper b-value. The use of simulation-based approaches for experiment design is interesting and should be further studied, but there is a need for improvements on computational efficiency or availability of more computational power such that fewer simplifications need to be made.
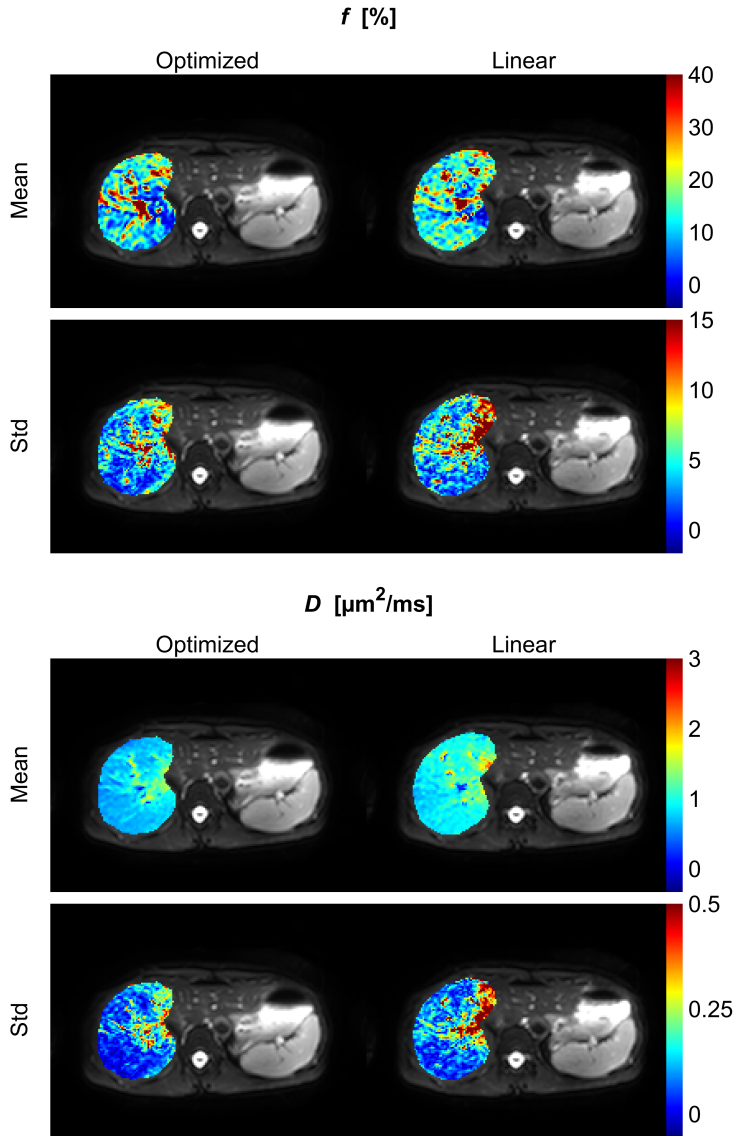
Figure 7: Voxelwise mean and standard deviation (std) of IVIM parameter maps from four repeated examinations of a healthy volunteer. The median std in the right part of the liver (colored region) with an optimized/linear b-value scheme was 0.115/0.147 µm^2/ms and 5.1/5.8 % for D and f, respectively. The variability of D and f was thus reduced by 22 and 12 %, respectively, by the use of the optimized b-value scheme in this example. Adapted from Paper III, Figure S14

Analysis of IVIM tumor parameter maps

This chapter is mainly related to Paper IV and partly to Paper II.

In Paper II, the ability of D and f to differentiate between tumor and healthy liver was studied.

In Paper IV, clustering based on Gaussian mixture models with IVIM parameter maps as input were used to identify tumor subregions. The identified subregions were compared with maps of proliferative activity derived from histological analysis.

Quantitative imaging, such as IVIM, shows great potential for tumor characterization [66]. By mapping physiologically relevant parameters it is possible to gain information on potentially interesting spatial variations within the tumor. Even so, most studies on tumors utilizing quantitative imaging only analyze parameter values that are averaged across the entire tumor [17]. To account for intratumor heterogeneity a couple of methods have been developed. These are mainly based on either describing the distribution of parameter values within the tumor, i.e. histogram or texture analysis, or partitioning the tumor into smaller regions, which are analyzed separately.

Methods for intratumor parameter analysis

Histogram and texture analysis

Histogram and texture analysis are methods based on extracting mathematical descriptions of the distribution of data. In histogram analysis no spatial information is considered, instead all voxel data from a tumor is pooled and a number of descriptives are used to summarize the

distribution of values. Typical descriptives include measures of central tendency (mean, median, mode), spread (variance, interquartile range), higher order metrics (skewness, kurtosis) and others (quantiles). In texture analysis, the variation between neighboring voxels is considered. Typical descriptives in this case are local and angular versions of correlation and entropy.

Histogram and texture analysis has shown great promise in many applications [67]. They are easy to understand methodologically and straight-forward to apply. However, higher order descriptives such as skewness and kurtosis are not obviously translated to a specific biological state, thereby resulting in a lack of interpretability [67, 68].

Region-based analysis

Instead of describing the distribution of parameter values within the tumor, one can choose to divide the tumor into subregions such that each subregion is relatively homogeneous and easy to describe [17].

One such alternative is to divide the tumor based on prior assumptions on its structure. A number of concentric ring-shaped regions with different distance from the center of the tumor can, for example, be defined [69, 70]. This approach can give insight to tumor physiology in different parts and provides a method that is easy to understand and describe. However, unless the tumor growth and development is purely radial, some degree of lost sensitivity due to averaging is inherent. Mismatch between rings and actual borders between functional regions is also a potential issue since statistics derived from nearby rings may become highly correlated, which complicates subsequent analysis [70].

Another alternative is to divide the tumor based on prior assumptions on the parameter values [71], for example, by setting some threshold parameter value to divide voxels into two groups. A similar approach, which is somewhat more data-driven, is to base such a threshold on the distribution of data, for example, a specific quantile. It is, however, less obvious why such a threshold would be biologically relevant.

A more fully data-driven approach is to partition the voxels within the tumor based on some kind of clustering [72]. Such an approach avoids the need for predefined thresholds or metrics. It can handle fairly complicated distributions and can in many cases easily be translated into a multiparametric situation in contrast to simple threshold-

based approaches where multidimensional thresholds may be nontrivial to define. It should, however, be noted that this kind of approach, where identification of tumor subregions is derived from the data itself, is primarily applicable to studies of new therapies, tumors, MRI methods or others, with relatively small sample sizes and with little or no a priori knowledge available. For a clinical setting where single patients are of interest, e.g., to provide personalized treatment evaluation, it is likely better to have predefined classification models trained and validated on large cohorts.

Cluster-based methods

The typical approach for cluster-based methods for identification of tumor subregions is to pool all voxel data from all tumors in all subjects and then perform a cluster analysis on the complete data set, as illustrated in Figure 8. The clustering result can then be transformed back to the individual tumors by identifying the cluster membership of each individual voxel.

Most studies aiming towards identification of tumor subregions based on clustering have used either k-means clustering or Gaussian mixture models. The k-means clustering is a hard clustering, i.e. voxels are only allowed to belong to a single cluster. k-means clustering is computationally efficient and the most commonly used clustering algorithm for identification of tumor subregions [72–80], but can be hampered if the distribution of data does not show very distinct clusters. In some recent studies, Gaussian mixture models (GMM) have been used [81–84]. GMM is, in contrast to k-means, a soft clustering algorithm, which means that voxels are assigned probabilities of belonging to each cluster. The probability for voxel i to belong to cluster k is given by:

$$P(x_i = k | \boldsymbol{y}_i) = \frac{P(\boldsymbol{y}_i | x_i = k) P(x_i = k)}{\sum_k P(\boldsymbol{y}_i | x_i = k) P(x_i = k)} \tag{15}$$

where $\boldsymbol{y}_i$ is a vector of data, that is D, f and D^* for data from the biexponential IVIM model, and x_i is the (unknown) class of voxel i [85].

$$P(\boldsymbol{y}_i | x_i = k) = \frac{1}{\sqrt{2\pi^d |\boldsymbol{\Sigma}_k|}} \exp\left[-\frac{1}{2}(\boldsymbol{y}_i - \boldsymbol{\mu}_k)^T \boldsymbol{\Sigma}_k^{-1}(\boldsymbol{y}_i - \boldsymbol{\mu}_k)\right] \tag{16}$$

where $\boldsymbol{\mu}_k$ and $\boldsymbol{\Sigma}_k$ are the mean vector and covariance matrix of cluster k, respectively, d is the number of dimensions, i.e. three when $\boldsymbol{y}_i$ contains D, f and D^*, and T indicates transpose [85]. $P(x_i = k) = \phi_k$ is the prior probability of belonging to cluster k. GMM can be used in cases of overlapping clusters and naturally handles parameters that are on different scales.

Much attention has been focused on clustering based on vascular properties by the use of parameters or time courses from DCE MRI [75–81, 84, 86, 87]. However, some studies have also used ADC and T2 [72–74, 78, 88]. Both diffusion and perfusion MRI can provide information important for tumor evaluation [89]. Since the two techniques relate to fundamentally different biological processes, their information is likely complementary and therefore highly suitable as input to a multidimensional clustering algorithm. One example of the complementary nature of the diffusion and perfusion information was shown in Paper II where differentiation between tumor and healthy liver was substantially improved by the combined use of D and f compared with use of D or f alone. IVIM is a strong candidate for providing diffusion and perfusion information to a clustering algorithm, not only because there is no need for an exogenous contrast agent, but also since only a single imaging sequence is used. This means that the different parameter maps for a given tumor are all in the same geometrical space, which is needed for the clustering analysis. On the other hand, if, for example, DCE parameters were to be combined with, e.g., ADC, a nontrivial co-registration would be needed. To further complement the IVIM parameters, a possibility could be to use T2-extended IVIM [34]. In addition to D, f and D^*, it also provides T2 relaxation times for both compartments and compensates for relaxation effects on f.

In paper IV, clustering was performed with the GMM algorithm and input data containing D, f and D^* to obtain subregions in neuroendocrine tumors of the GOT1 tumor model [58]. Based on the apparent good quality of parameter maps obtained from Bayesian IVIM model fitting with lognormal prior parameter distributions seen in Paper I, that approach for IVIM parameter estimation was chosen. To better conform to distributions approximated by a sum of Gaussian distributions, the log transform was applied to all IVIM parameters before clustering. This transformation is not permitted by all methods for IVIM model fitting due to the possibility of parameter estimates equal to zero, e.g. f obtained from segmented fitting. However, in Paper IV it served as an important preprocessing step. When the trans-
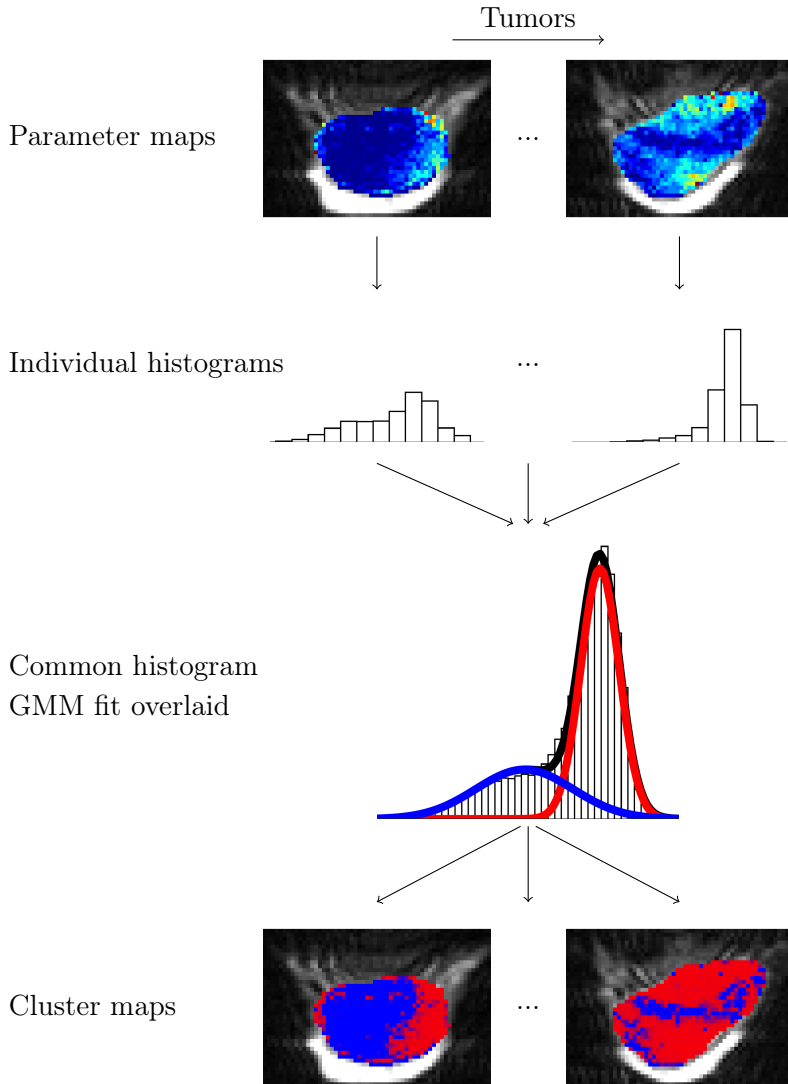
Figure 8: Flowchart showing how tumor subregions can be identified by Gaussian mixture modeling (GMM) based on data from parameter maps. The parameter data from each tumor is pooled to form a common parameter distribution. By fitting a GMM to the common parameter distribution the probability of belonging to a given class can be calculated for each voxel, which can be used to obtain maps of the clustering results. Adapted from Paper IV

formed IVIM parameter distributions were displayed in histograms, two relatively distinct clusters could be seen which both were well approximated by Gaussian distributions. This was confirmed by the cluster analysis which regarded two as the optimal number of classes. That number is specific for this study and in future work it is important to determine it for each specific situation.

It has previously been observed that inclusion of information from neighboring voxels can enhance the quality of the tumor subregions obtained from clustering [78]. Therefore, cluster analysis with a version of GMM that was altered to included information from neighboring voxels was also conducted in Paper IV. However, this only improved the quality marginally while the complexity of the analysis and computation time increased substantially. Whether spatial information should be included in the clustering or not is thus still an open question where the optimal choice likely depends on several factors including data quality, imaging techniques and tumor type.

Validation of clustering

When cluster-based methods are used it is important to note that they are solely driven by the data that is provided and the resulting subregions do not necessarily have any biological relevance. It is therefore necessary to evaluate the resulting subregions relative to some other aspect that is considered relevant for the particular tumor and situation. In most previous studies, the clustering results have either been related to some tissue characteristics from histological analysis [72, 73, 78] or evaluated as a predictor or measure for treatment effect [74, 87, 88].

Comparison of subregions obtained from cluster analysis with tissue characteristics derived from histological analysis provides a possibility to get a biological understanding of the obtained subregions. Since the characteristics of the clusters, i.e. their centers, are not known before the clustering analysis, it is preferable if the specific choice of histological parameters can be made after the clustering results are available. By doing so, it is possible to have hypotheses regarding the biological meaning of the clusters and choose staining techniques to obtain relevant histological parameters accordingly. Moreover, ideally the clusters should be compared with combinations of histological parameters or some histological parameter that is not directly comparable with a single MR parameter. The reasoning behind

this strategy is that the clustering is based on combinations of MR derived parameters and therefore the histological counterpart should be chosen to reflect the clustering results rather than any individual MR derived parameter. One such example that has been employed several times is to classify regions as viable tumor or necrosis based on hematoxylin and eosin staining, sometimes along with other complementary stainings, to compare with the subregions obtained from cluster analysis [72, 73, 78].

In Paper IV, the two obtained clusters were characterized by either high perfusion and low diffusion or low perfusion and somewhat higher diffusion. Based on the assumptions that the level of perfusion indicates availability of oxygen and nutrients and that measures of tissue water diffusion relates to cell density, it was hypothesized that the obtained subregions had different levels of proliferative activity. To assess the proliferative activity, index maps were derived from histological sections subject to Ki-67 staining. When the cluster maps were compared with the proliferation index maps a high degree of agreement could be seen, both regarding size and spatial similarity. The results thus confirm that IVIM based clustering has the potential to provide biologically relevant tumor subregions, but also more generally that IVIM parameters contain information potentially important for tumor tissue evaluation.

If the tumors are imaged at multiple time points, which are all included in the cluster analysis, it is possible to follow the development of subregions over time [76]. This could, for example, be of interest after some treatment has been given. It is then possible to extract longitudinal information such as size, average parameter value or even more complicated metrics from each subregion separately. The extracted information can then potentially be used as a measure or predictor for treatment outcome. Such a comparison with treatment effect is often the objective of a study, but ideally a histological analysis is also performed in order to improve the interpretability of the results [72, 73, 76, 88].

Conclusions

This thesis provides several methodological improvements related to intravoxel incoherent motion (IVIM) analysis. Specifically, it was shown that:

- choice of prior distribution and central tendency measure influence the performance of Bayesian IVIM model fitting and can have a large impact on the parameter estimates (Paper I). For analysis restricted to the parameters D and f the segmented IVIM model fitting is preferable (Paper II)

- optimization of b-value schemes has the ability to reduce estimation uncertainty of D and f substantially. Optimization of b-value schemes was enabled by development of a framework specific for estimation of D and f. The obtained optimized b-value schemes contained three unique b-values (Paper III)

- clustering using Gaussian mixture models based on IVIM parameter maps is able to identify tumor subregions, which correspond well with proliferative activity (Paper IV)

Altogether, the results of this thesis emphasize the importance of optimization of measurement and analysis methods for IVIM, and show that IVIM has a great potential to provide imaging biomarkers in e.g. cancer imaging.

Future aspects

IVIM is currently transitioning into clinical practice with analysis tools becoming available on several commercial platforms [90, 91]. However, if IVIM is to become a routine procedure in the clinic, consensus on imaging protocols and parameter estimation approaches is needed. Otherwise, interpretation and comparisons of parameter maps may be obscured by methodological differences. The results of this thesis and other work on IVIM methodology can serve as a basis for such a consensus.

During the last years, major methodological extensions have been proposed for IVIM, both regarding modeling and methods for diffusion encoding. To obtain more information and to better describe the diffusion weighted signal, it has been suggested to use an extended model for the diffusion compartment [92]. In that particular study, the kurtosis model was used, but any model that describes the curvature of the signal-vs-b curve would in principle apply [93]. More advanced methods for diffusion encoding, such as variable flow encoding, have also been proposed to better characterize the perfusion compartment [18, 20]. Including IVIM in the paradigm of multidimensional diffusion MRI has the potential to improve information output as well as robustness for IVIM analysis [94]. However, the increased complexity regarding both modeling and diffusion encoding necessitates studies on what approaches that actually provide important additional information and under which conditions. Optimization of acquisition parameters will be required and development of specialized estimation approaches may also be needed.

Future efforts should also be aimed at improved understanding of the origin of the IVIM signal. The physical origin can, for example, be studied by the use of complementary MRI techniques, while the biological interpretation can be strengthened by comparison with, for example, histological samples. Interesting results were shown in a re-

cent study where ASL with variable post labeling delay was combined with diffusion weighting to study how the blood signal is affected by diffusion weighting at different levels in the vessel tree [95]. In another study, the perfusion fraction was shown to be correlated with microvessel density as derived from histological analysis [96]. With the results of studies like these an increased understanding of the origin of the signal can be gained and the relation of IVIM to other perfusion techniques can be better understood. This can help in future development of the IVIM technique and to determine in which applications IVIM will give clinically relevant information.

Acknowledgements

References

[1] Erwin L Hahn. "Spin Echoes". In: *Physical Review* 80:4 (1950), pp. 580–594.

[2] Edward O Stejskal and John E Tanner. "Spin Diffusion Measurements: Spin Echoes in the Presence of a Time-Dependent Field Gradient". In: *The Journal of Chemical Physics* 42:1 (1965), pp. 288–292.

[3] Denis Le Bihan et al. "MR imaging of intravoxel incoherent motions: application to diffusion and perfusion in neurologic disorders." In: *Radiology* 161 (1986), pp. 401–407.

[4] Denis Le Bihan et al. "Separation of diffusion and perfusion in intravoxel incoherent motion MR imaging". In: *Radiology* 168:2 (1988), pp. 497–505.

[5] Anwar R Padhani et al. "Diffusion-Weighted Magnetic Resonance Imaging as a Cancer Biomarker: Consensus and Recommendations". In: *Neoplasia* 11:2 (2009), pp. 102–125.

[6] James P B O'Connor et al. "DCE-MRI biomarkers in the clinical evaluation of antiangiogenic and vascular disrupting agents". In: *British Journal of Cancer* 96:2 (2007), pp. 189–195.

[7] Andreas Lemke et al. "Toward an optimal distribution of b values for intravoxel incoherent motion imaging". In: *Magnetic Resonance Imaging* 29:6 (2011), pp. 766–776.

[8] Sebastiano Barbieri et al. "Impact of the calculation algorithm on biexponential fitting of diffusion-weighted MRI in upper abdominal organs". In: *Magnetic Resonance in Medicine* 75:5 (2016), pp. 2175–2184.

[9]   Harri Merisaari et al. "Fitting Methods for Intravoxel Incoherent Motion Imaging of Prostate Cancer on Region of Interest Level: Repeatability and Gleason Score Prediction". In: *Magnetic Resonance in Medicine* 77 (2017), pp. 1249–1264.

[10]   Yoshitaka Bito, Satoshi Hirata, and Etsuji Yamamoto. "Optimum Gradient Factors for Apparent Diffusion Coefficient Measurements". In: *Proceedings of the 3rd Annual Meeting of ISMRM*. Nice, France, 1995, p. 913.

[11]   Daniel C Alexander. "A General Framework for Experiment Design in Diffusion MRI and Its Application in Measuring Direct Tissue-Microstructure Features". In: *Magnetic Resonance in Medicine* 60 (2008), pp. 439–448.

[12]   Benjamin Leporq et al. "Optimization of Intra-voxel Incoherent Motion Imaging at 3.0 Tesla for Fast Liver Examination". In: *Journal of Magnetic Resonance Imaging* 41 (2015), pp. 1209–1217.

[13]   Björn Lampinen et al. "Optimal Experimental Design for Filter Exchange Imaging: Apparent Exchange Rate Measurements in the Healthy Brain and in Intracranial Tumors". In: *Magnetic Resonance in Medicine* 77:3 (2017), pp. 1104–1114.

[14]   Peter T. While et al. "Relative enhanced diffusivity: noise sensitivity, protocol optimization, and the relation to intravoxel incoherent motion". In: *Magnetic Resonance Materials in Physics, Biology and Medicine* 31:3 (2018), pp. 425–438.

[15]   Emma M. Meeus et al. "Rapid measurement of intravoxel incoherent motion (IVIM) derived perfusion fraction for clinical magnetic resonance imaging". In: *Magnetic Resonance Materials in Physics, Biology and Medicine* 31:2 (2018), pp. 269–283.

[16]   Mami Iima and Denis Le Bihan. "Clinical Intravoxel Incoherent Motion and Diffusion MR Imaging: Past, Present, and Future". In: *Radiology* 278 (2016), pp. 13–32.

[17]   James P.B. O'Connor et al. "Imaging intratumor heterogeneity: Role in therapy response, resistance, and clinical outcome". In: *Clinical Cancer Research* 21:2 (2015), pp. 249–257.

[18]   André Ahlgren et al. "Quantification of microcirculatory parameters by joint analysis of flow-compensated and non-flow-compensated intravoxel incoherent motion (IVIM) data". In: *NMR in Biomedicine* 29:5 (2016), pp. 640–649.

[19]   Denis Le Bihan. "What can we see with IVIM MRI?" In: *NeuroImage* DOI: `10.1016/J.NEUROIMAGE.2017.12.062` (2017).

[20]   Andreas Wetscherek, Bram Stieltjes, and Frederik Bernd Laun. "Flow-compensated intravoxel incoherent motion diffusion imaging". In: *Magnetic Resonance in Medicine* 74:2 (2015), pp. 410–419.

[21]   Richard P. Kennan et al. "A general model of microcirculatory blood flow effects in gradient sensitized MRI". In: *Medical Physics* 21:4 (1994), pp. 539–545.

[22]   Julien Sénégas et al. "Towards organ-specific b-values for the IVIM-based quantification of ADC: in vivo evaluation in the liver". In: *Proceedings of the 20th Annual Meeting of ISMRM*. Melbourne, Australia, 2012, p. 1891.

[23]   Qing Yuan et al. "A Simplified Intravoxel Incoherent Motion Model for Diffusion Weighted Imaging in Prostate Cancer Evaluation : Comparison with Monoexponential and Biexponential Models". In: *Proceedings of the 23rd Annual Meeting of ISMRM*. Toronto, Canada, 2015, p. 3019.

[24]   Qing Yuan et al. "Quantitative Diffusion-Weighted Imaging and Dynamic Contrast-Enhanced Characterization of the Index Lesion With Multiparametric MRI in Prostate Cancer Patients". In: *Journal of Magnetic Resonance Imaging* 45:3 (2017), pp. 908–916.

[25]   Denis Le Bihan and Robert Turner. "The capillary network: a link between ivim and classical perfusion". In: *Magnetic Resonance in Medicine* 27:1 (1992), pp. 171–178.

[26]   Christian Federau. "Intravoxel incoherent motion MRI as a means to measure in vivo perfusion: A review of the evidence". In: *NMR in Biomedicine* 30:11 (2017), pp. 1–15.

[27]   Ronnie Wirestam et al. "Perfusion-related parameters in intravoxel incoherent motion MR imaging compared with CBV and CBF measured by dynamic susceptibility-contrast MR technique". In: *Acta Radiologica* 42:2 (2001), pp. 123–128.

[28]   Noriyuki Fujima et al. "Intravoxel incoherent motion diffusion-weighted imaging in head and neck squamous cell carcinoma: Assessment of perfusion-related parameters compared to dynamic contrast-enhanced MRI". In: *Magnetic Resonance Imaging* 32:10 (2014), pp. 1206–1213.

[29] C Federau et al. "Perfusion measurement in brain gliomas with intravoxel incoherent motion MRI." In: *American journal of neuroradiology* 35:2 (2014), pp. 256–262.

[30] Wen-Chau Wu et al. "Caveat of measuring perfusion indexes using intravoxel incoherent motion magnetic resonance imaging in the human brain". In: *European Radiology* 25:8 (2015), pp. 2485–2492.

[31] Jignesh Patel et al. "Diagnosis of cirrhosis with intravoxel incoherent motion diffusion MRI and dynamic contrast-enhanced MRI alone and in combination: Preliminary experience". In: *Journal of Magnetic Resonance Imaging* 31:3 (2010), pp. 589–600.

[32] Sotirios Bisdas et al. "Correlative assessment of tumor microcirculation using contrast-enhanced perfusion MRI and intravoxel incoherent motion diffusion-weighted MRI: is there a link between them?" In: *NMR in Biomedicine* 27:10 (2014), pp. 1184–1191.

[33] Sonja Stieb et al. "Non-parametric intravoxel incoherent motion analysis in patients with intracranial lesions: Test-retest reliability and correlation with arterial spin labeling". In: *NeuroImage: Clinical* 11 (2016), pp. 780–788.

[34] Neil P Jerome et al. "Extended T2-IVIM model for correction of TE dependence of pseudo-diffusion volume fraction in clinical diffusion-weighted magnetic resonance imaging". In: *Physics in Medicine and Biology* 61:24 (2016), pp. 667–680.

[35] Anna Scherman Rydhög. "Diffusion-encoded MRI for assessment of structure and microcirculation: aspects of q-space imaging and improved IVIM modelling". PhD thesis. 2017.

[36] W T Dixon. "Separation of diffusion and perfusion in intravoxel incoherent motion MR imaging: a modest proposal with tremendous potential." In: *Radiology* 168:2 (1988), pp. 566–567.

[37] A. Luciani et al. "Liver Cirrhosis : Intravoxel Incoherent Motion MR Imaging". In: *Radiology* 249:3 (2008), pp. 891–899.

[38] Denis Le Bihan. "Intravoxel Incoherent Motion Perfusion MR Imaging: A Wake-Up Call". In: *Radiology* 249:3 (2008), pp. 748–752.

[39] C. Federau et al. "Intravoxel incoherent motion perfusion imaging in acute stroke: initial clinical experience". In: *Neuroradiology* 56:8 (2014), pp. 629–635.

[40] Y. Yao et al. "Intravoxel incoherent motion diffusion-weighted imaging in stroke patients: initial clinical experience". In: *Clinical Radiology* 71:9 (2016), pp. 11–16.

[41] Sungmin Woo et al. "Intravoxel incoherent motion diffusion-weighted MR imaging of hepatocellular carcinoma: correlation with enhancement degree and histologic grade." In: *Radiology* 270:3 (2014), pp. 758–767.

[42] Koung Mi Kang et al. "Intravoxel Incoherent Motion Diffusion-weighted MR Imaging for Characterization of Focal Pancreatic Lesions". In: *Radiology* 270:2 (2014), pp. 444–453.

[43] Gene Young Cho et al. "Evaluation of breast cancer using intravoxel incoherent motion (IVIM) histogram analysis: comparison with malignant status, histological subtype, and molecular prognostic factors". In: *European Radiology* 26:8 (2016), pp. 2547–2558.

[44] Håkon Gudbjartsson and Samuel Patz. "The Rician Distribution of Noisy MRI Data". In: *Magnetic Resonance in Medicine* 34:6 (1995), pp. 910–914.

[45] John A. Rice. *Mathematical statistics and data analysis*. 2007.

[46] James Pekar, Chrit T W Moonen, and Peter C M van Zijl. "On the precision of diffusion / perfusion imaging by gradient sensitization". In: *Magnetic Resonance in Medicine* 23 (1992), pp. 122–129.

[47] Hyo Jung Park et al. "Intravoxel incoherent motion diffusion-weighted MRI of the abdomen: The effect of fitting algorithms on the accuracy and reliability of the parameters". In: *Journal of Magnetic Resonance Imaging* 45:6 (2017), pp. 1637–1647.

[48] Emma M. Meeus et al. "Evaluation of intravoxel incoherent motion fitting methods in low-perfused tissue". In: *Journal of Magnetic Resonance Imaging* 45:5 (2017), pp. 1325–1334.

[49] Shiteng Suo et al. "Intravoxel incoherent motion diffusion-weighted MR imaging of breast cancer at 3.0 tesla: Comparison of different curve-fitting methods". In: *Journal of Magnetic Resonance Imaging* 42:2 (2015), pp. 362–370.

[50] Gene Young Cho et al. "Comparison of fitting methods and b-value sampling strategies for intravoxel incoherent motion in breast cancer". In: *Magnetic Resonance in Medicine* 74:4 (2015), pp. 1077–1085.

[51] Jeffrey J Neil and G Larry Bretthorst. "On the use of Bayesian probability theory for analysis of exponential decay data: an example taken from intravoxel incoherent motion experiments". In: *Magnetic Resonance in Medicine* 29 (1993), pp. 642–647.

[52] Thomas W Okell et al. "A Kinetic Model for Vessel-Encoded Dynamic Angiography with Arterial Spin Labeling". In: *Magnetic Resonance in Medicine* 68 (2012), pp. 969–979.

[53] Hadrien A Dyvorne et al. "Diffusion-weighted imaging of the liver with multiple b values: effect of diffusion gradient polarity and breathing acquisition on image quality and intravoxel incoherent motion parameters–a pilot study." In: *Radiology* 266:3 (2013), pp. 920–929.

[54] Moti Freiman et al. "Reliable estimation of incoherent motion parametric maps from diffusion-weighted MRI using fusion bootstrap moves". In: *Medical Image Analysis* 17:3 (2013), pp. 325–336.

[55] Matthew R Orton et al. "Improved Intravoxel Incoherent Motion Analysis of Diffusion Weighted Imaging by Data Driven Bayesian Modeling". In: *Magnetic Resonance in Medicine* 71 (2014), pp. 411–420.

[56] Anna S Rydhög et al. "Intravoxel incoherent motion (IVIM) imaging at different magnetic fi eld strengths: What is feasible?" In: *Magnetic Resonance Imaging* 32:10 (2014), pp. 1247–1258.

[57] Peter T While. "A Comparative Simulation Study of Bayesian Fitting Approaches to Intravoxel Incoherent Motion Modeling in Diffusion-Weighted MRI". In: *Magnetic Resonance in Medicine* 78:6 (2017), pp. 2373–2387.

[58] Lars Kölby et al. "A transplantable human carcinoid as model for somatostatin receptor-mediated and amine transporter-mediated radionuclide uptake". In: *American Journal of Pathology* 158:2 (2001), pp. 745–755.

[59] Jeff L Zhang et al. "Optimization of b-value Sampling for Diffusion-Weighted Imaging of the Kidney". In: *Magnetic Resonance in Medicine* 67 (2012), pp. 89–97.

[60] Manfred Eis and Mathias Hoehn-Berlage. "Correction of gradient crosstalk and optimization of measurement parameters in diffusion MR imaging". In: *Journal of Magnetic Resonance* 107 (1995), pp. 222–234.

[61] Da Xing et al. "Optimised Diffusion-Weighting for Measurement of Apparent Diffusion Coefficient (ADC) in Human Brain". In: *Magnetic Resonance Imaging* 15:7 (1997), pp. 771–784.

[62] D K Jones, M A Horsfield, and A Simmons. "Optimal Strategies for Measuring Diffusion in Anisotropic Systems by Magnetic Resonance Imaging". In: *Magnetic Resonance in Medicine* 42 (1999), pp. 515–525.

[63] Oscar Brihuega-Moreno, Frank P Heese, and Laurance D Hall. "Optimization of Diffusion Measurements Using Cramer-Rao Lower Bound Theory and Its Application to Articular Cartilage". In: *Magnetic Resonance Imaging* 50 (2003), pp. 1069–1076.

[64] Dirk H.J. Poot et al. "Optimal Experimental Design for Diffusion Kurtosis Imaging". In: *IEEE Transactions on Medical Imaging* 29:3 (2010), pp. 819–829.

[65] Oscar Gustafsson, Maria Ljungberg, and Göran Starck. "Can Cramer-Rao Lower Bound be used to find optimal b-values for IVIM?" In: *Proceedings of the 24th Annual Meeting of ISMRM*. Singapore, 2016, p. 2043.

[66] Claude D. Marcus et al. "Imaging techniques to evaluate the response to treatment in oncology: Current standards and perspectives". In: *Critical Reviews in Oncology/Hematology* 72:3 (2009), pp. 217–238.

[67] Nathalie Just. "Improving tumour heterogeneity MRI assessment with histograms." In: *British journal of cancer* 111:12 (2014), pp. 2205–2213.

[68] Lejla Alic, Wiro J. Niessen, and Jifke F. Veenland. "Quantification of heterogeneity as a biomarker in tumor imaging: A systematic review". In: *PLoS ONE* 9:10 (2014), pp. 1–15.

[69] Jon-Vidar Gaustad et al. "Intratumor heterogeneity in blood perfusion in orthotopic human melanoma xenografts assessed by dynamic contrast-enhanced magnetic resonance imaging". In: *Journal of Magnetic Resonance Imaging* 21:6 (2005), pp. 792–800.

[70] Mikael Montelius et al. "Identification of Potential MR-Derived Biomarkers for Tumor Tissue Response to 177Lu-Octreotate Therapy in an Animal Model of Small Intestine Neuroendocrine Tumor." In: *Translational oncology* 11:2 (2018), pp. 193–204.

[71] David Checkley et al. "Use of dynamic contrast-enhanced MRI to evaluate acute treatment with ZD6474, a VEGF signalling inhibitor, in PC-3 prostate tumours". In: *British Journal of Cancer* 89 (2003), pp. 1889–1895.

[72] Richard. A D Carano et al. "Quantification of Tumor Tissue Populations by Multispectral Analysis". In: *Magnetic Resonance in Medicine* 51:3 (2004), pp. 542–551.

[73] Erica C. Henning et al. "Multispectral quantification of tissue types in a RIF-1 tumor model with histological validation. Part I". In: *Magnetic Resonance in Medicine* 57 (2007), pp. 501–512.

[74] Leanne R. Berry et al. "Quantification of viable tumor microvascular characteristics by multispectral analysis". In: *Magnetic Resonance in Medicine* 60:1 (2008), pp. 64–72.

[75] Erlend K. F. Andersen et al. "Pharmacokinetic analysis and k-means clustering of DCEMR images for radiotherapy outcome prediction of advanced cervical cancers". In: *Acta Oncologica* 50:6 (2011), pp. 859–865.

[76] Igor Jacobs et al. "Cluster analysis of DCE-MRI data identifies regional tracer-kinetic changes after tumor treatment with high intensity focused ultrasound". In: *NMR in Biomedicine* 28:11 (2015), pp. 1443–1454.

[77] Dario Livio Longo et al. "Cluster analysis of quantitative parametric maps from DCE-MRI: Application in evaluating heterogeneity of tumor response to antiangiogenic treatment". In: *Magnetic Resonance Imaging* 33:6 (2015), pp. 725–736.

[78] Prateek Katiyar et al. "A Novel Unsupervised Segmentation Approach Quantifies Tumor Tissue Populations Using Multiparametric MRI: First Results with Histological Validation". In: *Molecular Imaging and Biology* 19 (2016), pp. 391–397.

[79] Turid Torheim et al. "Cluster analysis of dynamic contrast enhanced MRI reveals tumor subregions related to locoregional relapse for cervical cancer patients". In: *Acta Oncologica* 55:11 (2016), pp. 1294–1298.

[80]   Jia Wu et al. "Intratumor partitioning and texture analysis of dynamic contrast-enhanced (DCE)-MRI identifies relevant tumor subregions to predict pathological response of breast cancer to neoadjuvant chemotherapy". In: *Journal of Magnetic Resonance Imaging* 44:5 (2016), pp. 1107–1115.

[81]   So Hyan Han et al. "Gaussian mixture model-based classification of dynamic contrast enhanced MRI data for identifying diverse tumor microenvironments: preliminary results". In: *NMR in Biomedicine* 26 (2013), pp. 519–532.

[82]   Nicolas Coquery et al. "Microvascular MRI and Unsupervised Clustering Yields Histology-Resembling Images in Two Rat Models of Glioma". In: *Journal of Cerebral Blood Flow & Metabolism* 34:8 (2014), pp. 1354–1362.

[83]   Mathew R. Divine et al. "A Population-Based Gaussian Mixture Model Incorporating 18F-FDG PET and Diffusion-Weighted MRI Quantifies Tumor Tissue Classes". In: *Journal of Nuclear Medicine* 57:3 (2016), pp. 473–479.

[84]   Adam K. Featherstone et al. "Data-driven mapping of hypoxia-related tumor heterogeneity using DCE-MRI and OE-MRI". In: *Magnetic Resonance in Medicine* 79:4 (2017), pp. 2236–2245.

[85]   Christopher M. Bishop. *Pattern recognition and machine learning.* 2006.

[86]   Umberto Castellani et al. "DCE-MRI data analysis for cancer area classification". In: *Methods of Information in Medicine* 48:3 (2009), pp. 248–253.

[87]   Peng Wang et al. "An approach to identify, from DCE MRI, significant subvolumes of tumors related to outcomes in advanced head-and-neck cancer". In: *Medical Physics* 39:8 (2012), pp. 5277–5285.

[88]   Erica C. Henning et al. "Multispectral tissue characterization in a RIF-1 tumor model: Monitoring the ADC and T2 responses to single-dose radiotherapy. Part II". In: *Magnetic Resonance in Medicine* 57 (2007), pp. 513–519.

[89]   Sonia P. Li and Anwar R. Padhani. "Tumor response assessments with diffusion and perfusion MRI". In: *Journal of Magnetic Resonance Imaging* 35:4 (2012), pp. 745–763.

[90]   Philips Healthcare. *IntelliSpace Portal 10*. 20180730. URL: `https://www.philips.co.uk/healthcare/product/HC881102/intellispace-portal-10-advanced-visualization` Accessed: 20180730.

[91]   Olea Medical. *Olea Sphere 3.0*. 20180730. URL: `https://www.olea-medical.com/en/olea-sphere-3-0/additionnal-plug-ins/ivim/` Accessed: 20180730.

[92]   Mami Iima et al. "Quantitative non-gaussian diffusion and intravoxel incoherent motion magnetic resonance imaging Differentiation of malignant and benign breast lesions". In: *Investigative Radiology* 50:4 (2015), pp. 205–211.

[93]   Jean-Pierre Cercueil et al. "Intravoxel incoherent motion diffusion-weighted imaging in the liver: comparison of mono-, bi- and tri-exponential modelling at 3.0-T". In: *European Radiology* 25:6 (2015), pp. 1541–1550.

[94]   Daniel Topgaard. "Multidimensional diffusion MRI". In: *Journal of Magnetic Resonance* 275 (2017), pp. 98–113.

[95]   Xingxing Zhang et al. "Comparison of perfusion signal acquired by arterial spin labeling–prepared intravoxel incoherent motion (IVIM) MRI and conventional IVIM MRI to unravel the origin of the IVIM signal". In: *Magnetic Resonance in Medicine* 79:2 (2018), pp. 723–729.

[96]   Hye Jeong Lee et al. "Tumor perfusion-related parameter of diffusion-weighted magnetic resonance imaging: Correlation with histological microvessel density". In: *Magnetic Resonance in Medicine* 71:4 (2014), pp. 1554–1558.